Magnetic Hyperthermia efficiency and ^{1}H-NMR Relaxation Properties of IronOxide/Paclitaxel loaded PLGA Nanoparticles.

Maria R. Ruggiero[a,b,] Simonetta. Geninatti Crich[a], Elisabetta Sieni[c], Paolo Sgarbossa[c], Michele Forzan[c] , Eleonora Cavallari[a] , Rachele Stefania[a], Fabrizio Dughiero[c], Silvio Aime[a]*

[a]University of Torino, Department of Molecular Biotechnology and Health Sciences, via Nizza 52, Torino, Italy.

[b]SAET S.p.A Via Torino, 213 10040 - Leinì (To), Italy.

[c]University of Padova, Department of Industrial Engineering, via Gradenigo 6/a, Padova, Italy.

Corresponding Author*: e-mail simonetta.geninatti@unito.it

Online supplementary data available from….

ABSTRACT

Magnetic Iron Oxide Nanoparticles (Fe-NPs) can be exploited in biomedicine as agents for Magnetic Fluid Hyperthermia treatments (MFH) and contrast enhancers in Magnetic Resonance Imaging (MRI). New, oleate covered, Iron Oxide particles have been prepared either by coprecipitation or thermal decomposition methods and incorporated into PLGA (PLGA=Poly(lactic-co-glycolic acid) nanoparticles (PLGA-Fe-NPs) to improve their biocompatibility and "in vivo" stability. Moreover, the PLGA-Fe-NPs have been loaded with Paclitaxel to pursue an MFH triggered drug release. Remarkably, it has been found that the nanoparticles formulations are characterized by peculiar ^{1}H-NMRD profiles that directly correlate with their heating potential when exposed to an alternating magnetic field. By prolonging the magnetic field exposure to 30min a significant drug release was observed for PLGA-Fe-NPs in the case of the larger sized magnetic nanoparticles. Furthermore, the immobilization of lipophilic Fe-NPs in PLGA-NPs allowed to maintain Néel relaxation as the dominant relaxation contribution also in the presence of large iron oxides cores (diameter of 15-20nm) with the advantage of preserve their efficiency when they are entrapped in the intracellular environment. The herein reported results show that NMRD profiles are a useful tool for anticipating heating capabilities of Fe-NPs designed for MFH applications.

1. INTRODUCTION

Nanoscale stimuli-responsive systems are under intense scrutiny with the aim of providing therapeutic treatments characterized by limited unspecific cytotoxic effects. Among different physical triggers, large alternating magnetic fields (AMF) enable the conversion of magnetic energy into heat by using magnetic nanoparticles that generate localized hyperthermia named magneto fluid hyperthermia (MFH)[1,2]. It has been suggested that this methodology can be exploited in cancer therapy either directly or/and for thermally activated drug release. However, despite the promising results, iron oxide based MFH has not yet been translated to routine clinical practice for the following main reasons: i) the low heating power of the clinically approved iron oxide nanoparticles; ii) their limited ability to target tumour cells; iii) their inhomogeneous distribution in the tumour tissue. In order to reach the concentration needed for a successful treatment, MFH treatments have to rely on the direct injection of magnetic nanoparticles into the tumour. Many efforts are currently devoted to the preparation of more efficient iron oxide particles to make MFH a competitive therapy in particular to treat metastasis and spreading tumour masses[3,4]. To date all magnetic nanoparticles used in vivo are composed of magnetite (Fe_3O_4) and maghemite (γ-Fe_2O_3) due to their low toxicity and their known biodistribution and metabolism[5]. To prevent agglomeration, particles are coated with protective shells (e.g. polymers like dextran, starch, aminosilane, and polyethylene glycol). Different mechanisms are responsible for the thermal energy generated by magnetic nanoparticles in the presence of an alternating magnetic field. They are related to the magnetic properties of the nanoparticles (i.e. the overall magnetization (M_s), and the effective anisotropy constant (K_{eff}) that are strictly dependent on their size, shape, coating and chemical composition[6,7]. Briefly, heat dissipation arises from the delayed response to the time dependent applied magnetic field. It depends on the relaxation of the magnetic moment that may occur through e-ither the spin fluctuations within the crystal (Néel) or the rotation of the particle itself (Brownian)[8-10]. The optimal frequency of the AC magnetic field that should be used to obtain the maximum heat dissipation depends on the size of the magnetic nanoparticle and on the viscosity of the medium[11-12].

The effective relaxation time (τ) of the magnetic particles is defined as

$$\frac{1}{\tau} = \frac{1}{\tau_N} + \frac{1}{\tau_B} \qquad (1)$$

where τ_N and τ_B are the Néel and Brownian magnetic relaxation times, respectively. The shorter relaxation time determines the dominant relaxation mechanism.

τ_B and τ_N magnetic relaxation times of a particle are given by the following equations[8]:

$$\tau_B = \frac{3\eta V_H}{kT} \tag{2}$$

$$\tau_{NArr} = \tau_0 \, exp \frac{E_{A.Arr}}{kT} \tag{3}$$

$$\tau_{N,VF} = \tau_{0,VF} exp \frac{E_{A,VF}}{k(T-T_0)} \tag{4}$$

Where η is the viscosity, V_H the hydrodynamic particle volume, k the Boltzmann constant, T the temperature, $\tau_0 = 10^{-9}$ s, E_A is the average energy barrier for the reversal of the magnetization and T_0 is a phenomenological parameter estimated by the Vogel-Fulcher model.

τ_N is described by the Arrhenius equation (Equation 3) or by the modified heuristic Vogel-Fulcher model[13] (Equation 4) in the presence of not-interacting or interacting particles, respectively.

The relative contribution arising from Néel and Brown relaxation processes depend on the particle size, shape and chemical characteristics. The Néel time has an exponential dependence on magnetic anisotropy and particle volume, whereas the Brownian correlation time varies linearly with particle volume and solvent viscosity[14]. Whereas, Néel relaxation is not influenced by viscosity of the medium[11,15], Brownian relaxation is influenced markedly by this parameter. It follows that if the viscosity of the medium is high or the particle reorientational motion is reduced as a consequence of particles aggregation or entrapment in intracellular compartments (endosomes, lysosomes), the heat dissipated by the Brownian mechanism decreases dramatically[8]. Furthermore, theoretical and experimental results strongly suggest that highly efficient intracellular hyperthermia modality can be achieved by exploiting the Néel rather than the Brownian relaxation. Thus to improve the efficiency of the MFH treatment, and to establish a robust relationship between "in vitro" and "in vivo" experiments it is essential to use particles that relax through Néel relaxation. Moreover, it is crucial for the development of MFH to rely on analytical methods able to characterize new magnetic nanoparticles and to predict their heating

capacity in physiological conditions. For example, the theory behind the calculation of the anisotropy constant from magnetic measurements often neglects interparticle interactions, so that the obtained values reported in the literature show often marked discrepancies among studies dealing with similar particles[16].

In this study, the MFH properties of newly prepared iron oxide nanoparticles (Fe-NPs) with a diameter ranging from about 5 to 18 nm, coated with oleate moieties and prepared either by co-precipitation or thermal decomposition methods have been evaluated in relation to their size and shape. The selected synthetic methods, apart from being two of the most used techniques for the production of iron oxide nanoparticles, proved to be easy and reliable routes for the synthesis of nanoparticles with both regular (thermal decomposition) and irregular (co-precipitation) shape with diameters ranging from 5 to 18 nm. This would allow for the study of their MFH properties in relation to their morphology in terms of shape and size distribution. Since the magnetic nanoparticles are stabilized toward aggregation by coating with oleate molecules, they are completely insoluble in water. In order to improve Fe-NPs bioavailability they were incorporated into PLGA (Poly(lactic-co-glycolic acid) nanoparticles (PLGA-Fe-NPs)[17-19]. The incorporation of magnetic nanoparticles inside PLGA-Fe-NPs has many advantages[3,20-23] i) it improves the magnetic nanoparticles stability and bioavailability; ii) it allows their efficient dispersion in water; iii) it avoids their aggregation; iv) it hampers the Brownian relaxation by blocking magnetic nanoparticles inside the PLGA-Fe-NPs solid core thus allowing Néel relaxation, also in the presence of larger particles. The results from the "in vitro" characterization can be immediately used for foreseeing the "in vivo" behavior. The correlation between field dependence of the longitudinal relaxation rate (R_{1obs}), described by the so-called Nuclear Magnetic Resonance Dispersion (NMRD) profile, for different types of nanoparticles and their heating power has been investigated. For iron oxide particles the inner sphere contribution to the water protons relaxation is negligible whereas the outer sphere term is the dominant one[14,24,25]. Outer sphere relaxation is essentially due to the diffusion of the water protons near the local variable magnetic field generated by the paramagnetic ion. Thus, by analyzing the dipolar interaction between proton spins and the magnetic moment of the nanocrystal it is possible to extrapolate important information about the magnetic nanoparticles namely, their average distance of minimum approach to the metal ion (r_{NMRD} in Table 3), their specific magnetization M_s, their anisotropy energy E_a, and their Néel relaxation time τ_N that determine the heating potential of the magnetic nanoparticles. Moreover,

PLGA-Fe-NPs have been loaded also with an anticancer hydrophobic drug currently used in the treatment of ovarian and breast cancer (Paclitaxel, PTX) in view of developing MFH triggered drug release [26,27].

2. EXPERIMENTAL SECTION

2.1 Synthesis of magnetic iron oxide nanoparticles

Iron(III) acetilacetonate ([Fe(acaca)$_3$]), iron(III) chloride hexahydrate (FeCl$_3$·6H$_2$O), iron(II) chloride tetrahydrate (FeCl$_2$·4H$_2$O), oleyl amine, oleyc acid, 1,2-tetradecanediol, ammonium hydroxide (25% aq. sol.), diphenyl ether, dibenzyl ether, ethanol, *n*-hexane were purchased by Aldrich. All reagents were used as provided by the manufacturer without further purification. The nanoparticles of the series C1 and C12 have been synthesised according to a slight modification of the method proposed by Sun et al[28]. A solution of iron(III) acetylacetonate (5 mmol) in diphenyl (C1) or dibenzyl (C12) ether (50 ml) has been treated with 1,2-tetradecanediol (25 mmol), oleylamine (15 mmol) and oleic acid (15 mmol) at 200°C for 1 h and then at reflux under nitrogen atmosphere and vigorous mechanical stirring. After cooling at room temperature and washing with ethanol, the nanoparticles have been separated magnetically and dispersed in *n*-hexane. Nanoparticles of the series C5 have been synthesized according to the method proposed by Ghasemi et al.[29] by coprecipitation from a solution of iron(II) and iron(III) chloride (25 and 50 mmol respectively) in deionized water (150 ml) with ammonium hydroxide as a base. After adding the base under vigorous mechanical stirring until pH reaches 11, oleic acid (5 % vol.) is added to the dark suspension and the temperature is raised to 60°C for 30 min. The black-brown precipitate is separated magnetically, washed several times with water and finally dispersed in *n*-hexane.

2.2 PLGA-Fe-NPs preparation

Poly(D,L-lactide-co-glicolide) (PLGA) RG 502H 50:50, average molecular weight (Mw) 30000-60000Da, and Poly(vinyl alcohol), Mw 31000−50000 Da (98−99% hydrolyzed) was provided by Sigma-Aldrich and Paclitaxel was purchased from Aurisco Pharmaceutical Limited (China).

PLGA-Fe-NPs were obtained using an oil-in-water emulsion solvent extraction method. The emulsion was prepared dissolving 100 mg of PLGA, 1 mg of Paclitaxel (PTX) and Iron oxide nanoparticles (5 mg of Iron) in 2 mL of chloroform; this solution was called phase 1. Phase 2 consisted of 3% w/v PVA aqueous solution (4 mL). Phase 1 was added into phase 2 drop to drop and sonicated for 300sec at 100% of power. The final emulsion was transferred to a 100 ml round-bottom flask and put into a rotary evaporator (at 740 mmHg and 30 rpm) for 150 min to remove the organic solvent. Non-entrapped drug was removed by dialysis (molecular weight cutoff of 14 000 Da) carried out at 4 °C against an isotonic NaCl/Hepes buffer (HBS). The excess of PVA was removed by washing the emulsion with vivaspin filters (Sartorius) (cutoff of 1×10^6 Da) by centrifugation at 5000 rpm for 3 times with 20ml of buffer HBS.

The amount of Fe entrapped in PLGA-Fe-NPs was determined by using inductively coupled plasma mass spectrometry (ICP-MS; element-2; Thermo-Finnigan, Rodano (MI), Italy). Sample digestion was performed with concentrated HNO_3 (70%, 1 ml) under microwave heating

(Milestone MicroSYNTH Microwave labstation). The hydrated mean diameter of PLGA-Fe-NPs was determined using a dynamic light scattering (DLS) Malvern Zetasizer 3000HS (Malvern, U.K.). All the samples were analysed at 25°C in filtered PBS buffer (cut-off point: 100 nm; pH 7).

2.3 Determination of Paclitaxel concentration in nanoparticles

The drug loading efficiency was determined in duplicate by HPLC (Alliance Waters 2695, Milford, Massachusetts, USA). The mobile phase consisted in acetonitrile/water (50:50). The reverse phase was X-Bridge C18 5µm. The flow rate was set 1.0ml/min and the detection wavelength is 227 nm. The HPLC was calibrated with standard solutions of 10 to 150 µg/ml of PTX dissolved in acetonitrile (R^2 = 0,99984). The limit of quantification was 0.6 ng/ml. The samples were freeze-dry and sonicated in ultrasonic bath with chloroform for 30 min. After centrifugation at 5000 rpm for 10 min and evaporation of chloroform, they were sonicated again with acetonitrile for 15min and then analysed by HPLC. The encapsulation efficiency was defined by the ratio of measured and initial amount of PTX encapsulated in nanoparticles.

2.4 $^1H/T_1$ NMRD Profiles

The $1/T_1$ nuclear magnetic relaxation dispersion profiles of water protons were measured over a continuum of magnetic field strength from 0.00024 to 0.5 T (corresponding to 0.01–20 MHz proton Larmor frequency), on the fast field cycling (Stelar Spinmaster FFC 2000 relaxometer) equipped with a resistive low inductance air cored solenoid, made in silver and used in Fast Field Cycling NMR relaxometers[30]. The relaxometer operates under complete computer control with an absolute uncertainty in the $1/T_1$ values of ±1%. The typical field sequences used were the NP sequence between 20 and 8 MHz and PP sequence between 8 and 0.01 MHz. The observation field was set at 16 MHz. T_1 was determined by the saturation recovery method. 16 values of delay (τ) between pulses have been used. The number of averaged experiments was 2. Water proton T_1 measurements at fixed frequency were carried out on a Stelar Spin Master Spectrometer [Stelar S.n.c., Mede (PV), Italy] operating in the range from 20 to 80 MHz, by means of the inversion recovery method (16 delays (τ) values, two averages). The reproducibility of the T_1 data was ± 5%.

2.5 TEM analysis.

The Transmission Electron Microscopy (TEM) analysis (TECNAI FEI G2 microscope) has been used to analyze the morphology of the nanoparticles highlights both the PLGA-Fe-NPs shell and the magnetic nanoparticle content.

2.6 Heating by means of time-varying magnetic field Studies.

The device to apply the time-varying magnetic field to magnetic nanoparticles is composed by a voltage generator EASYHEAT 8310 LI connected to a cylindrical inductor. The EASYHEAT 8310 LI supplies the inductor with a voltage up to 700 V_{rms} in a frequency range between 150 and 400 kHz. The copper inductor is a cylindrical solenoid with 7 turns, an internal diameter of 8 cm and a length of 15 cm. An image of the measurement set-up is in Figure 4. The sample is logged in Teflon container where a 5 ml glass vial is screwed to the cup of the container (Figure 4). The temperature is measured by means of an Optocom Fotemp-1H thermometer with a TS3/2 fiber optic. The fiber optic is inserted in the 5 ml glass vial by means of a hole in the center of the cup. The temperature is sampled with a time step of 1 s.

The inductor supplied by a time varying current of 400 A at 177 kHz is able to generates a magnetic field with a pick value close to 18 kA/m (corresponding to a magnetic flux density in air of 22.6

mT). The experiments have been carried out for a time 5 min or for 30 min. During each experiment the temperature has been acquired as a function of the time.

2.7 Stability and in vitro drug release

Paclitaxel loaded nanoparticles, at concentration of 2.3 μg/ml in 2 ml of PBS, were transferred to dialysis bags (MWCO: 10000 Da) and placed in 50 mL of PBS with stirring at 110 rpm/37 °C. At determined time intervals (6, 24 and 48 hours), the environmental buffer solution was removed and replaced with fresh PBS. The removed buffer was freeze-dry and sonicated in ultrasonic bath with 10 ml of chloroform for 30 min. After centrifugation at 5000rpm for 10min and evaporation of chloroform, they were sonicated again in ultrasonic bath with 0.2 ml of acetonitrile for 15min and then analyzed by HPLC, as described above.

3. RESULTS AND DISCUSSION

Iron oxide magnetic nanoparticles, used for the preparation of the PLGA nanocomposites, were obtained by two synthetic procedures, namely: i) co-precipitation in basic conditions from an iron(II/III) chlorides containing solution (sample C5) and ii) thermal decomposition of an organometallic derivative of iron(III) in the presence of oleic acid and oleylamine as surfactants (samples C1 and C12). Magnetic nanoparticles size and morphology were obtained by TEM analysis (Figure 1). For each samples the average size was evaluated using ImageJ software and the average particle sizes are shown in Table 1. As expected the nanoparticles obtained by co-precipitation (C5) show a higher dispersity and a larger average diameter compared to the samples obtained by thermal decomposition. The presence of a relatively small fraction (about 17%) of particles with larger diameter (18.0 ± 1.7 nm) has been taken into account for both NMRD and MFH studies. Thermal decomposition can produce very regular spherical nanoparticles at the lower boiling temperature of phenyl ether (Figure 1, C1) while, moving to benzyl ether the higher reflux temperature led to the formation of irregularly shaped nanoparticles (Figure 1, C12) characterized by an increased size and polydispersity. In fact, as shown in Figure 1, C12 samples contains a fraction (13%) of particles with larger diameter (15.6 ± 3.8) and with a not spherical shape (triangle, diamond) that markedly affected the magnetic properties of the sample as described below.

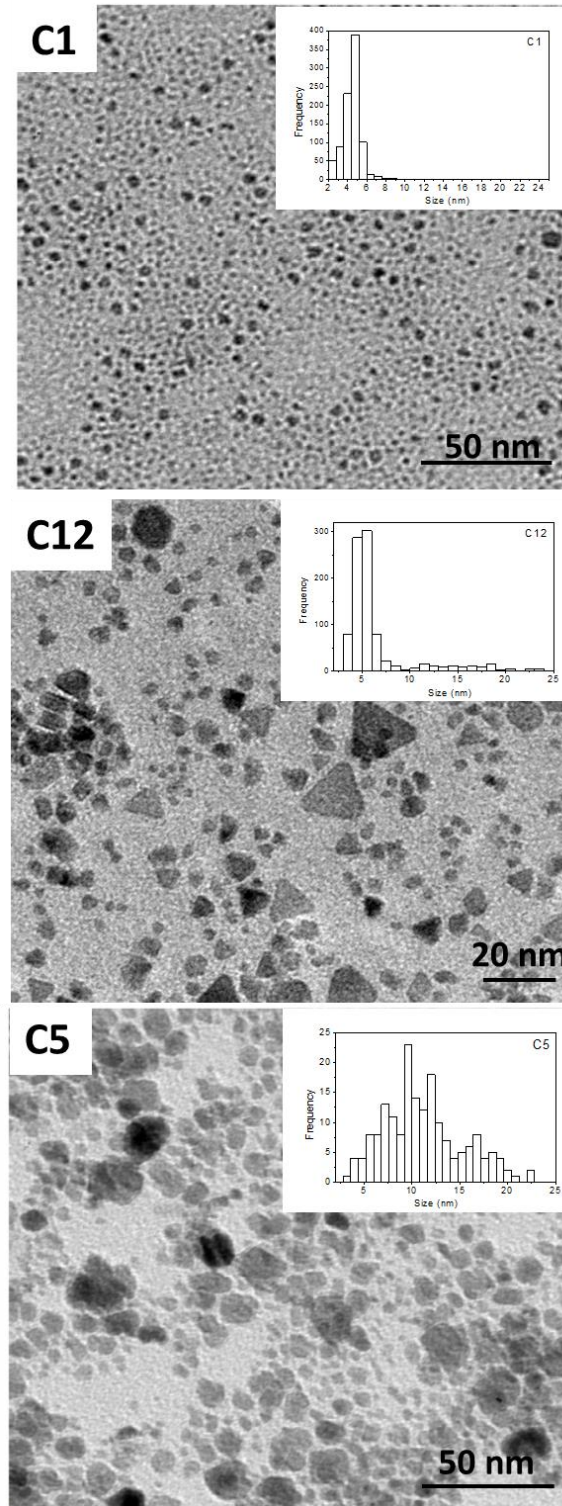| Fe-NPs	Diameter (nm) (TEM)	Preparation method
C1	5.2 ± 0.9	Thermal decomposition
C5	9.7 ± 2.8 (83%); 18.0 ±1.7(17%)	Co-precipitation
C12	5.1 ± 1.0 (87%); 15.6 ± 3.8 (13%)	Thermal decomposition

Table 1. Metal core diameters of Fe-NPs measured by TEM.

Figure 1. TEM images of the different magnetic nanoparticles with their relative histograms of size distribution.

3.1 PLGA-Fe-NPs preparation and characterization.

PLGA-Fe-NPs were obtained by the o/w emulsion solvent extraction method[31]. The organic phase was prepared by dissolving PLGA RG 502H, Fe-NPs, and paclitaxel in chloroform. The water phase was a poly(vinyl alcohol) (PVA) aqueous solution. PVA is the most commonly used emulsifier for the preparation of PLGA-NPs because it yields particles that are relatively uniform, small sized, and easy to be re-dispersed in water[32]. To obtain PLGA nanoparticles the organic phase was added to the aqueous phase, and the resulting mixture was extensively sonicated. The nanospheres were prepared by slow organic solvent evaporation of the o/w emulsion. The encapsulation yields in PLGA-Fe-NPs are reported in Table 2. The amount of iron in PLGA-Fe-NPs was determined by ICP-MS whereas paclitaxel concentration was determined by HPLC using a reverse phase column[33].The differences in % loaded Fe are the consequence of the different particles re-dispersion efficiency in the organic solvent. The average hydrodynamic diameters of PLGA-Fe-NPs were obtained by dynamic light scattering (DLS) measurements, and they are reported in Table 1. The longitudinal (r_1) and transverse (r_2) millimolar relaxivities (21.5 MHz, 25 °C) of the PLGA-Fe-NPs are reported in Table 2.

PLGA-Fe-NPs	%Fe	%PTX	Diameter/DLS	r_{1p} [mM^{-1}s^{-1}]	r_{2p} [mM^{-1}s^{-1}]
PLGA-C1	96±2	-	121±2 nm	3.7±0.9	175±30
PLGA-C5	68±9	40±12	164±12 nm	9.5±0.8	393±20
PLGA-C12	12±7	27 ± 5	159±7 nm	10.6±1.4	300±20

Table 2. PLGA-Fe-NPs composition; diameters (measured by Dynamic Light Scattering); r_{1p} and r_{2p} (measured at 21.5 MHz and T=25°C).

Figure 2 shows TEM images of the PLGA-Fe-NPs. The average diameter resulted to be about 80-90 nm whereas the hydrodynamic size measured by DLS was significantly larger (120-170 nm). This difference has been explained by the presence of a large solvation shell, typical of PLGA based nanoparticles, when dispersed in an aqueous medium[34]. The occurrence of this shell causes an overestimation of the hydrodynamic size.

Partial aggregation of the magnetic particles inside the PLGA core has been observed for PLGA-C5 and in minor extent, for PLGA-C12.
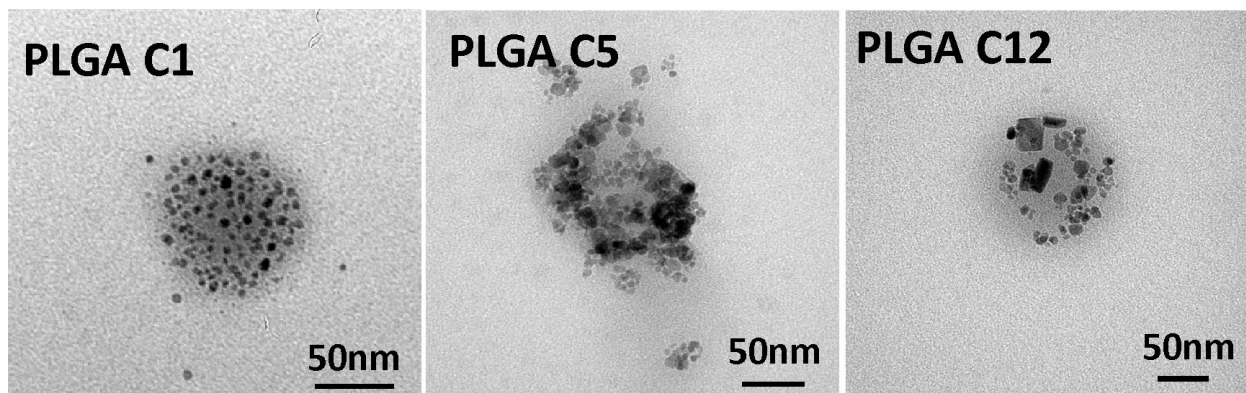

Figure 2. TEM images of PLGA-Fe-NPs

3.2 Relaxometric Properties of PLGA-Fe-NPs.

Figure 3 displays the T_1 magnetic field dependence (NMRD) of PLGA-Fe-NPs compared with Endorem (a commercially available SPIO particle used as MRI contrast agent). The shape of the curves is typical of the relaxation induced by superparamagnetic particles[14], i.e. the loading into the PLGA matrix seems not affecting the overall magnetic properties of the iron oxide particles. Differences in shapes of NMRD profiles are depending on the particle properties (size, clustering, Néel relaxation time and saturation magnetization). The water proton longitudinal relaxation arises from the dipolar interaction between the magnetic moments of water protons and the electron magnetic moment of the iron oxide particles and it is modulated by Néel relaxation (flip of the particle magnetic moment from different anisotropy directions) and water diffusion. Theories are available to describe relaxation for small and large particles[24,25]. At low magnetic fields, for

particles with a diameter > 15 nm, the high crystal anisotropy maintains the particle magnetic moment locked onto the anisotropy axis. Since they can flip from one easy direction to another, the relaxation can occur through either Néel relaxation or water diffusion. On the contrary, at high magnetic fields, the Néel relaxation is not possible since the magnetic moment is locked onto the magnetic field direction and the modulation is due to water diffusion (τ_D). For very small particles, characterized by a smaller anisotropy energy, the locking of the particle magnetization onto the anisotropy directions does not occur and Néel relaxation becomes irrelevant also at low magnetic fields. In this study, the longitudinal NMRD profiles have been fitted using the Roch's heuristic model[35] modified by Lascialfari et al[13] that has been developed for particle core diameter < 20 nm. Fitting equations were written using *Matlab* software (see supplementary information). For the fitting of C5 and C12 samples the TEM radius of larger diameter particles (Table 1) have been used.
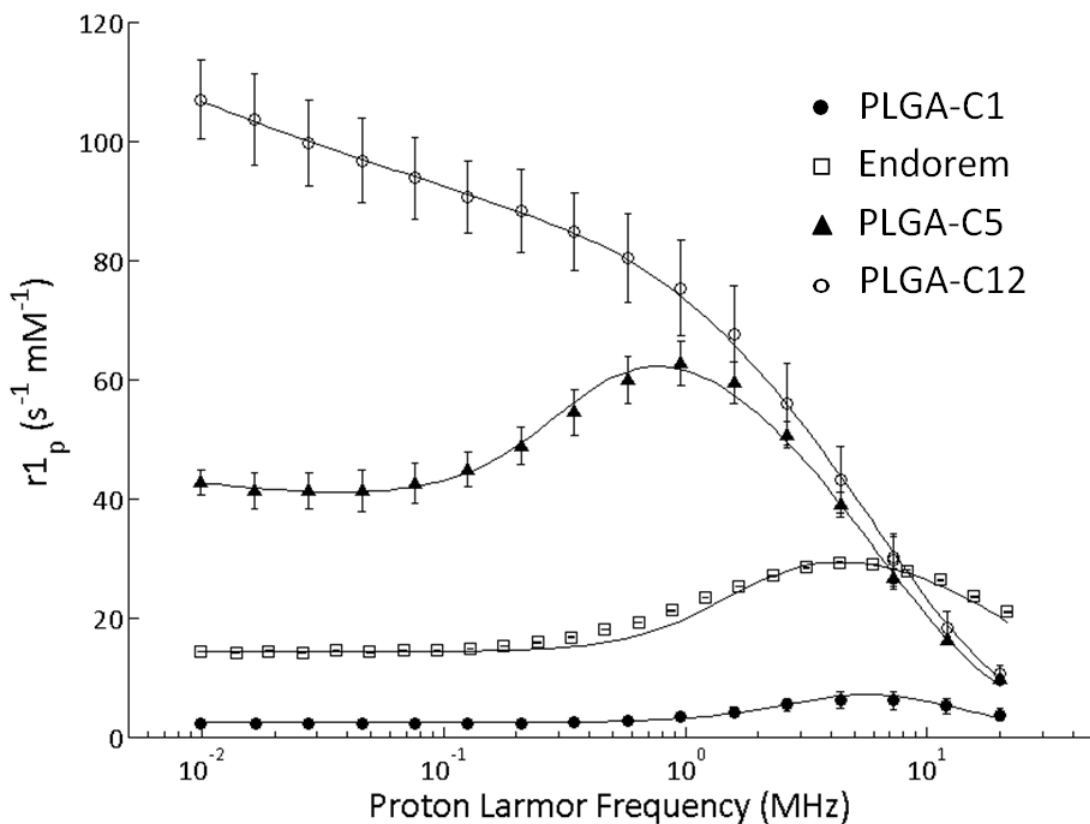

Figure 3. Profiles of 1/T$_1$ ^{1}H-NMRD (25°C and pH=7.4) of PLGA-Fe-NPs loaded with the different magnetic nanoparticles: C12 (○), C5 (▲), Endorem (□), and C1 (●). The solid lines

between data points are the result of the data analysis (see the equations in supplementary information). PLGA-Fe-NPs profiles are the average of 4 different preparations. Error bars represent the SD of the experimental data.

The relaxation rate at very low fields is directly proportional to the crystal anisotropy energy and particle volume. Figure 3 shows dramatic differences (C1<endorem<C5) in low field relaxation rates of PLGA loaded with magnetic particles. The observed behaviour reflects differences in crystal shape, τ_N and size of magnetic core from TEM images (Figure 2). Tentatively, the unexpected profile of PLGA loaded with C12 particles can be explained by the presence of ca. 13% of larger particles (15.6 ± 3.8 nm diameter) characterized by a not spherical shape. Apparently this fraction represents the dominant contribution to the observed NMRD profile. At high field the relaxation rate only depends on τ_D (translational correlation time) and the inflection point corresponds to the condition defined by $\omega_I \tau_D \sim 1$. Since $\tau_D = r^2/D$, where D is the water diffusion coefficient (2.3×10^{-5} cm^2/s) the determination of τ_D from the NMRD profile allows to estimate the distance of minimum approach (r_{NMRD}). Table 3 reports τ_N , τ_D,, Ms, and r obtained by the fitting of NMRD profiles for the different PLGA-Fe-NPs and Endorem. The hydrodynamic iron oxide core sizes derived from the NMRD profile are larger than those ones obtained by TEM but significantly smaller than the hydrodynamic sizes of the whole PLGA-Fe-NPs particles (80-90 and 120-170 nm by TEM and DLS, respectively). These effects result from the fitting procedure of the NMRD profiles, which depends on the distance of minimum approach of water molecules to the metal core whereas TEM data give the real size of the magnetic core. Being the magnetic particles embedded in the PLGA framework particles we can conclude that water can relatively freely diffuse inside this material and the free diffusion is inversely proportional to the PLGA-NPs size[30,36]. Since the r_{NMRD} appears independent by the TEM-measured size of the Fe-NPs, one can hypothesize than the observed relaxation rates are limited by the hindered water diffusion inside the PLGA matrix that it can be assumed to be analogous in the different PLGA-NP preparations.

PLGA-Fe-NPs	r_{TEM} [nm]	r_{NMRD} [nm]	τ_D [ns]	$M_{S,NMRD}$ [emu g^{-1}]	τ_N [s rad^{-1}]
PLGA-C1	2.6 ± 0.5	15.8 ± 0.8	108 ± 11	108 ± 20	$1.69 \pm 0.97 \times 10^{-9}$
Endorem	2.5 ± 0.5	6.35 ± 0.29	17.5 ± 1.6	98.5 ± 9.6	$3.7 \pm 1.2 \times 10^{-9}$
PLGA-C5	9.0 ± 0.9	13.2 ± 0.3	75.8 ± 3.9	62.1 ± 2.6	$2.73 \pm 0.48 \times 10^{-7}$
PLGA-C12	7.8 ± 1.9	13.9 ± 0.2	84.0 ± 2.6	64.9 ± 2.1	$10.95 \pm 4.05 \times 10^{-6}$

Table 3. Best fitting parameters obtained by the analysis of NMRD profiles of PLGA-Fe-NPs measured at 25°C. Radius particles have been compared with that obtained by TEM.

From the $1/T_1$ NMRD profile analysis it is possible to check the reproducibility of nanoparticle synthesis and to assess the parameters that influence MFH. On the other hand, from the measurement of transverse relaxivity (R_2) of PLGA-Fe-NPs suspensions it is possible to evaluate their efficiency as T_2* agents for MRI applications. In fact, iron oxide nanoparticles can be exploited both as contrast agents for MRI in T_2* weighted images and as therapeutics in MFH making them "ideal" theranostic agents. Table 2 shows that, as expected, highest values of R_2 (measured at 21.5MHz) have been obtained for particles with the largest diameter (PLGA-C5). As reported for the $1/T_1$ NMRD profiles analysis the R_2 are not dependent on the size of the whole PLGA nanoparticle (ca. 150-180nm) but only on the size of the magnetic core and the distance of minimum approach (r). The r_{2p} of PLGA-C5 and PLGA-C12 are particularly high, suggesting their use as promising T_2* MRI contrast agents.

3.3 Assessment of magnetic hyperthermia properties.

The PLGA-Fe-NPs were exposed to a time varying magnetic field (Figure 4) in order to evaluate their potential in generating magnetic hyperthermia. The temperature increase generated by heat

dissipation was recorded as a function of time of exposure to the AMF. The induction device[37-38] (Figure 4) used in this study was developed at the University of Padova and it is described in the experimental section.
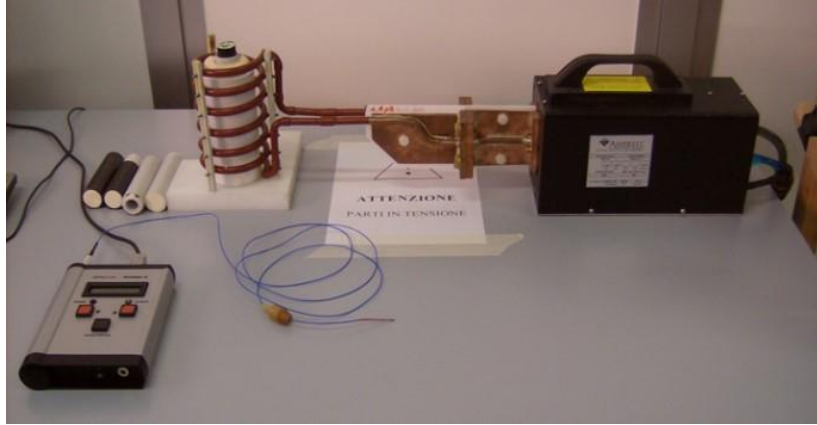

Figure 4. A photograph of the high-frequency induction device

Typically, heating efficiency of a material is reported in terms of the specific absorption rate (SAR) reported in equation (5), where C is the heat capacity of the suspension, m_{sample} is the mass of the sample, m_{iron} is the mass of iron, and ΔT is the initial slope of the time-dependent heating curve, respectively[11].

$$SAR = C \ \frac{m_{sample}}{m_{iron}} \frac{\Delta T}{\Delta t} \qquad\qquad (5)$$

While the SAR values can have a maximum point at a certain particle size, they are proportional to the initial magnetic susceptibility, frequency and strength of the applied field (H_0).

The time dependent temperature curves were fitted by using the phenomenological Box-Lucas equation. (Equation 6)

$$T(t) = A(1 - e^{-Bt}) \qquad\qquad (6)$$

This equation is often used to describe the AMF heating of iron oxide nanoparticles[39]. The product of the fitting parameters, A x B, is equivalent to the initial temperature rise ($\Delta T/\Delta t$) and it was used to calculate SAR values from equation (5).

The solutions were placed in an AC magnetic field of frequency ν = 1 77 kHz and amplitude H_0 = 18 kA/m, corresponding to a product $H_0 \nu$ = 2.4×10^9 A m^{-1} s^{-1} . This value is under the tolerance threshold estimated by Hergt and coworkers[40] for a small exposed region ($H_0 \nu < 5 \times 10^9$ A m^{-1} s^{-1}) in order to avoid the production of tissue heating due to induced eddy currents. Figure 5 shows the ΔT measured after a varying magnetic field exposure of 5min. PLGA loaded with C12 and C5 particles are significantly more efficient than the NPs loaded with smaller C1 ones.
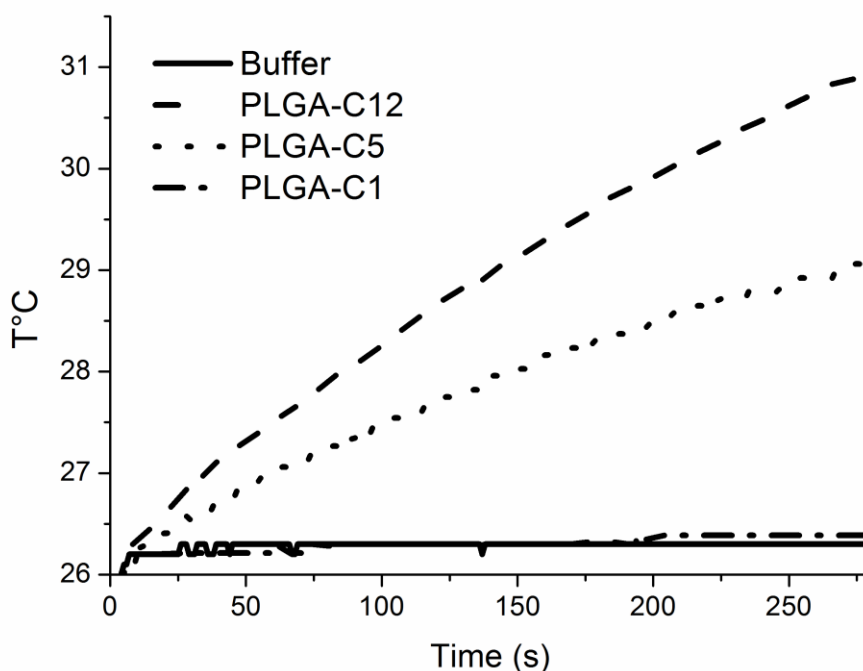

Figure 5. Temperature increase by magnetic heating of PLGA-Fe-NPs (time exposure 5min). The Fe concentration in all solutions was of 20.8 mM (determined by ICP-MS)

The observation is consistent with that reported by Lartigue et al[41], particles up to 7 nm do not produce significant heating under similar experimental conditions. From these results, one may surmise that, in PLGA-C12, the population with larger diameter (ca. 16 nm) represents the species

that give the dominant contribution to the observed temperature increase as reported above for the observed NMRD profile. Since there is an inverse proportionality between the maximum SAR values obtainable with a magnetic nanoparticle and the polydispersity of their size and shape[42,43], both C5 and C12 synthetic protocol will be improved to reduce the polydispersity of these particles and therefore to improve their heating efficiency.

Very interestingly, as shown in Figure 6A, there is a direct proportionality between SAR and r_{1p} (mM^{-1} s^{-1}) (as measured at very low magnetic fields, 0.01 MHz).
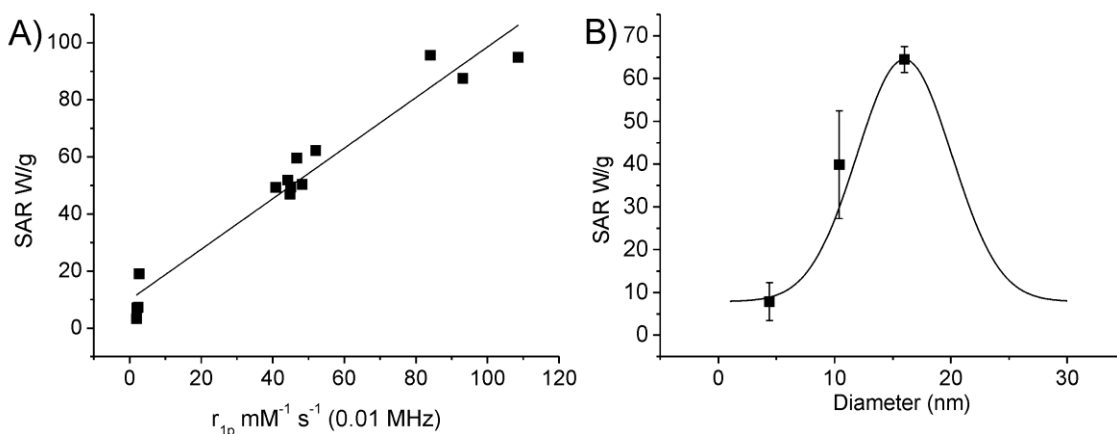

Figure 6. Plot of SAR values for the PLGA-Fe-NPs as a function of the relaxivity measured at low magnetic field (A) and of their size (B).

At low magnetic fields, the water proton relaxation rate, is directly proportional to the anisotropy energy. It follows that the magnetic properties of Fe-NPs embedded in PLGA-NPs are not affected by the global motion of the nanoparticle as they dissipate heat through Néel relaxation[8-9]. This observation is confirmed by the bell-shaped behavior of the SAR dependence on magnetic particle radius extrapolated by the NMRD profiles (Figure 6B) as theoretically estimated by M. Suto and coworkers[7].

3.4 "In vitro" Paclitaxel release triggered by MFH.

The loading of the PLGA-Fe-NPs with an antitumour drug (Paclitaxel) leads to a "theranostic" agent that combines hyperthermia generated cytotoxicity with chemotherapy. This combination may allow to reduce the amount of drug and to achieve the synergistic therapeutic effect in treating

cancers after a single or few administrations. PLGA has been loaded with paclitaxel and C5 or C12 NPs, respectively. Resulting PLGA-Fe-NPs have been exposed to the AMF for 30min. This exposure time allowed to reach a maximum external temperature increase of about 12°C for the more efficient PLGA-C12 system (Figure 7).
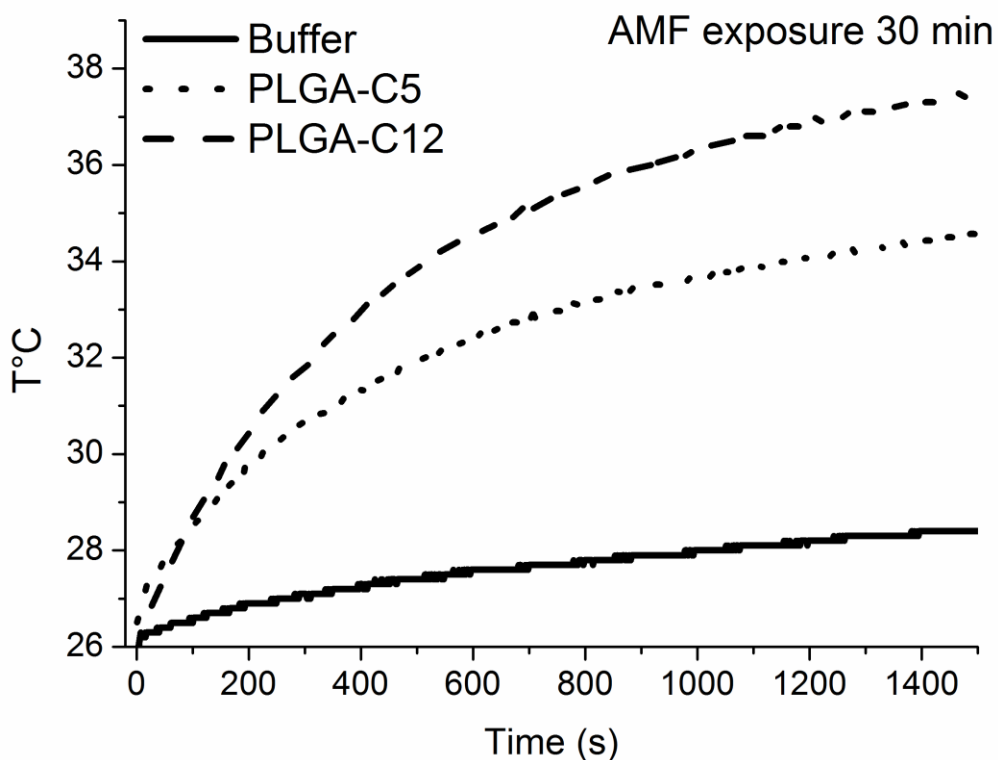

Figure 7. Temperature increase by magnetic heating brought by PLGA-C5 and PLGA-C12 systems (time exposure 30min). The Fe concentration in the NPs suspensions was of 20.8 mM (determined by ICP-MS)

In vitro Paclitaxel release from nanoparticles was estimated in Phosphate Buffer Saline (PBS) at 6, 24 and 48h after AMF exposure. Paclitaxel loaded nanoparticles (2,3 µg/ml) were diluted in PBS (2ml) and transferred to dialysis bags–placed in PBS (50ml) with magnetic stirring at 110 rpm/37 °C. At appropriate intervals, the buffer solution was replaced with fresh PBS, and the

concentration of the released Paclitaxel in the removed PBS was determined by HPLC. Figure 8 shows the amount of paclitaxel released by PLGA-Fe-NPs after 30min the AMF exposure is significantly higher than that measured on both control and on samples exposed to AMF only for 5min. The heat produced during the MFH treatment is sufficient to destabilize PLGA-Fe-NPs triggering their selective drug release. Since C12 and C5 have a high R_2/R_1 ratio they can be exploited as T_2^* MRI contrast agents able to report, in real time, their "in vivo" distribution. On the basis of the observed contrast enhancement it should be possible to find the most appropriate timing to initiate the MFH treatment.
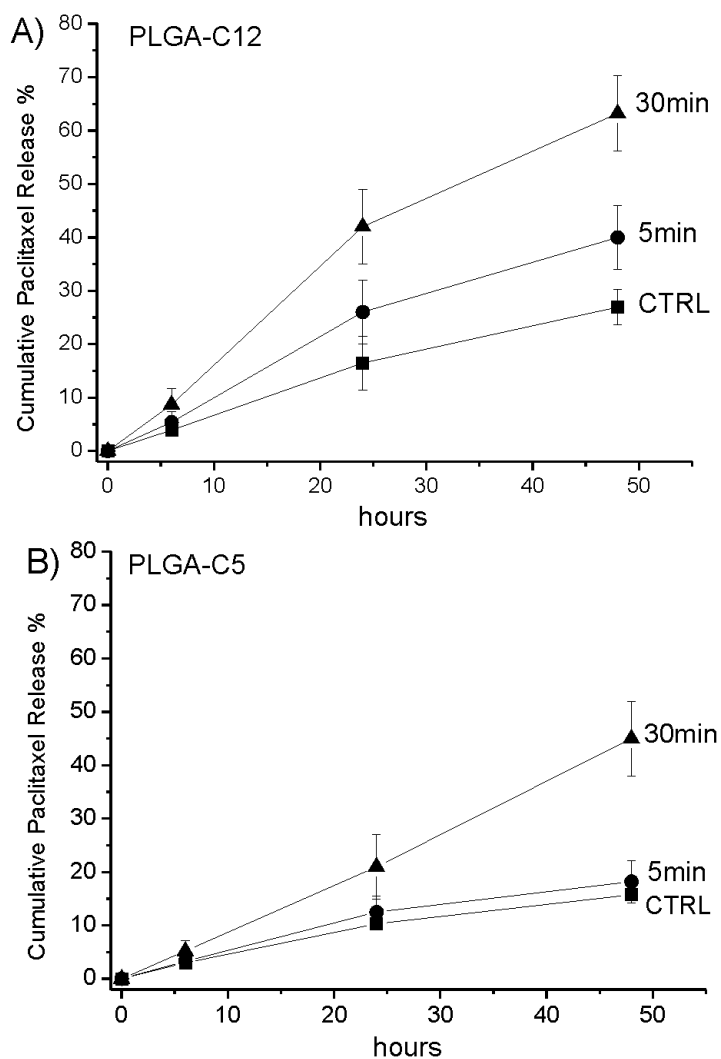
Figure 8. Cumulative Paclitaxel release measured at 37°C by HPLC for PLGA-C12 (A) and PLGA-C5 (B).

4. CONCLUSION

The herein reported results have shown that: i) PLGA is a good, biocompatible material to encapsulate iron oxide particles to yield stable NPs, easily suspended in aqueous solutions; ii) the PLGA-Fe-NPs NMRD profiles allow to predict their performance in both MRI and MFH applications; iii) the PLGA matrix does not hamper a free diffusion of water molecules at the surface of Fe-NPs; iv) the heating (by MFH) of PLGA-Fe-NPs loaded with Paclitaxel allows a triggered release of the drug from the NPs. Finally, new nanosystems loaded with Fe-NPs and Paclitaxel appear very promising systems for designing innovative "theranostic" applications.

REFERENCES

1) Hildebrandt,B, Wust, P, Ahlers, O, Dieing, A, Sreenivasa, G, Kerner, T, Felix, R, et al. 2002, *Critical reviews in oncology/hematology*, **43**, 33–56.

2) Krishnan, K.M, 2010, Biomedical Nanomagnetics: *IEEE Transactions on*, **46**, 2523–2558.

3) Goya, G.F, Asín, L, Ibarra, L.R, 2013, *International Journal of Hyperthermia*, **29**, 810–818.

4) Andreu, I, Natividad, E, Soloza´ bal, L, Roubeau, O, 2015, *ACS Nano*, **9**, 1408-19.

5) Laurent, S, Bridot, J.L, Vander Elst, L, Muller R.N, 2010, *Future Med Chem*. **2**, 427-49.

6) Rudolf, H, Dutz, S, Muller, R., Zeisberger, M., 2006, *Condens. Matter*, **18**, S2919–S2934.

7) Swati V. Jadhav,a Dipali S. Nikam,a Sawanta S. Mali,b Chang K. Hongb and

   Shivaji H. Pawar*a NewJ.Chem., 2014, 38, 3678

8) Suto, M, Hirota, Y, Mamiya, H, Fujita, A, Kasuya, R, Tohji, K, Jeyadevan, B, 2009, *Journal of Magnetism and Magnetic Materials,* **321,** 1493–1496.

9) Rosensweig, R.E. 2002, *J Magn Magn Mater*, **252**, 370-375.

10) Fortin, J.P, Wilhelm, C., Servais, JC, 2007, *J. Chem. Am. Soc.*, **129**, 2628-2635.

11) Fortin, J.P, Gazeau, F, Wilhelm, C, 2008, *Eur Biophys J* , **37**, 223–228.

12) Hiroaki, M, Balachandran, J, 2011, *Sci Rep.*, 1:**157,** 1-7.

13) Bordonali, L., Kalaivani, T.,Sabareesh, K.P.V., Innocenti, C., Fantechi, E., Sangregorio, C., Casula, M.F., Lartigue, L.,, Larionova, J., Guari, Y., Corti, M., Arosio, P., Lascialfari, A., 2013 *J. Phys: Condens. Matter*, **25**, 066008.

14) Laurent, S, Forge, D, Port, M, Roch, A, Robic, C, Vander Elst, L, Muller, R.N, 2008, *Chem. Rev*., **108,** 2064-110.

15) Kozissnik, B, Bohorquez, A.C, Dobson, J, Rinaldi, C, 2013, *Int J Hyperthermia*, **29**, 706-14.

16) Andreu, I, Natividad, E, Ravagli, C, Castroa, M, Baldi, G, 2014, *RSC Adv*, **4,** 28968–28977.

17) Makadia, H,K, Siegel, S, 2011, *Polymers*, **3**, 1377−1397.

18) Middleton, J.C, Tipton, A.J, *2*000, *Biomaterials*, **21**, 2335−2346.

19) Danhier, F, Ansorena E, Silva, J.M, Coco, E, Le Breton, A, Préat V, 2012, *Journal of Controlled Release*, **161**, 505–522.

20) Ngaboni Okassa, L.; Marchais, H.; Douziech-Eyrolles, L.; Cohen-Jonathan, S.; Souc´e, M.; Dubois, P.; Chourpa, I.; 2005, *International Journal of Pharmaceutics*, **302**, 187–196.

21) Wassel, R.A, Grady, B, Kopke, R.D, Dormera, K.J.; 2007, *Physicochem. Eng. Aspects*, **292**, 125–130.

22) Shen, J.M, Yin, T, Tian, X.Z., Gao, F.Y., Xu, S., 2013, *ACS Appl. Mater. Interfaces*, **5**, 7014−7024.

23) You Ling, Kun Wei, Yun Luo, Xin Gao, Shizhen Zhong Biomaterials 32 (2011) 7139-7150.

24) Gossuin, Y., Gillis, P., Hocq, A., Vuong, Q.L.;, Roch, A., 2009, Wiley *Interdiscip Rev Nanomed Nanobiotechnol*, **1**, 299-310.

25) Gossuin, Y., Disch, S., Vuong, Q.L., Gillis, P., Hermann, R.P., Park, J.H., Sailor, M.J., 2010, *Contrast Media Mol Imaging*, **5**, 318-22.

26) Cui, Y.; Xu, Q.; Chow, P,K.; Wang, D.; Wang C.H.; 2013, *Biomaterials*, **34**, 8511-20.

27) Hu, S.H, Liao, B.J., Chiang, C.S., Chen, P.J., Chen, I.W., Chen, S., 2012, *Adv Mater*, **24**, 3627-32.

28) Sun, S., Zeng, H. Robinson, D.B., Raoux, S., Rice, P.M., Wang, S.X., Li, G., 2004, *J. Am. Chem. Soc.*, **126**, 273–279.

29) Ghasemi, E., Mirhabibi, A., Edrissi, M., 2008, *Journal of Magnetism and Magnetic Materials*, **320**, 2635–2639.

30) Ferrante, G, Sykora, S, 2004 *Advanced in inorganic chemistry*, **57**, 405-470.

31) Mariano, R.N., Alberti, D., Cutrin, J.C., Geninatti Crich, S., Aime, S., 2014, *Mol. Pharmaceutics*, **11**, 4100−4106.

32) Sahooa, S.K., Panyama, J., Prabhaa, S., Labhasetwara, V., 2002, *J Controlled Release*, **82**, 105−114.

33) Danhiera, F., Lecouturiera, N., Vromana, B.C., Jérômeb, J. Marchand-Brynaertc, O. Ferond, V. Préata, 2009, *Journal of Controlled Release*, **5**, 11–17.

34) Carvalho Silva R. Muehlmann, LA, Rodrigues da Silava, J, De Bentes Azevedo, R, Madeira Lucci, C, 2014, *Microscopy Research and Technique*, **77**, 691–696.

35) Roch, A., Muller, R.N., Gillis, P., 1999, *J. Chem. Phys.*, **11**, 5403-5411.

36) Choi, S. W., Kwon, H. Y., Kim, W. S., Kim, J. H., 2002, *Colloids Surf.*, **201**, 283−289.

37) Bertani, R., Ceretta, F., Dughiero, F., Forzan, M., Gandin, V., Marzano, C., Michelin, R., Sgarbossa, P., Sieni, E., Spizzo, F., 2015, 6th European Conference of the International Federation for Medical and Biological Engineering, Lackovi, I, Vasic, D., A c. Springer International Publishing, **45**, 329–332.

38) Bertani,R., Ceretta, F., Di Barba, P., Forzan, M., Dughiero, F., Michelin, R., Sgarbossa, P., Sieni, E., Spizzo, F., 2015, *Eng. Comput*, **32**, 7.

39) Murase, K., Takata, H., Takeuchi, Y., Saito, S., 2013, *Physica Medica*, **29,** 624-630.

40) Hergt, R., Dutz, S., 2007, *Journal of Magnetism and Magnetic Materials*, **311**,187–192.

41) Lartigue, L., Innocenti, c., Kalaivani, T., Awwad, A., Sanchez Duque Mdel, M., Guari, Y., Larionova, J., Guérin, C., Montero, J.L., Barragan-Montero, V., Arosio, P., Lascialfari, a., Gatteschi, D., Sangregorio, C., 2011, *J Am Chem Soc*, **133**, 10459-72.

42) Reza Barati, M, Selomulya, C, Suzuki, K, 2014, *Journal of Applied Physics*, **115**, 17-22.

43) Gonzales-Weimuller, M, Zeisberger, M, Krishnan, KM, 2009*, Journal of Magnetism and Magnetic Materials*, **321**, 1947–1950.